

# Physicochemical Processes Occurring During the Formation of Cellulose Diacetate Membranes. Research of Criteria for Optimizing Membrane Performance. V. Cellulose Diacetate–Acetone–Water–Inorganic Salt Casting Solutions

C. LEMOYNE, C. FRIEDRICH, J. L. HALARY, C. NOËL, and L. MONNERIE, *Laboratoire de Physicochimie Structurale et Macromoléculaire, ESPCI, 75231 Paris Cedex 05, France*

## Synopsis

Consideration was given to the effects of casting conditions upon the performance and structure of membranes prepared from CA–acetone–water–inorganic salt solutions. Treating casting solutions as polymer–solvent–nonsolvent ternary systems, the data on equilibrium phase separation conditions were plotted in a triangular diagram for solutions containing  $\text{Al}(\text{NO}_3)_3$ ,  $\text{KSCN}$ ,  $\text{Mg}(\text{ClO}_4)_2$  or no additive. Measurements of casting solution viscosity, membrane thickness, freezing and nonfreezing water contents were used to supplement flux and retention data of membranes made by varying the inorganic salt and holding time in a systematic way. With the aid of scanning and transmission electron microscopy, it was concluded that membranes may consist of one, two, three, or four layers. The data and correlations obtained allow us to propose a mechanism of formation for each of these layers.

## INTRODUCTION

Studies have been carried out on the physicochemical processes occurring during the various phases of membrane preparation from cellulose diacetate–acetone–water–inorganic salt casting solutions. The results obtained so far make it possible to state the quantity of water required for polymer precipitation,<sup>1</sup> the speed of gelation,<sup>1</sup> and the effect of heat treatment on membrane properties.<sup>2</sup> The kinetics of acetone evaporation from films obtained by casting solutions of cellulose diacetate–acetone–water–inorganic salt have been also analyzed.<sup>3</sup>

Ever since the discovery of the skinned membranes by Loeb and Sourirajan,<sup>4</sup> there has been a great deal of effort to understand the mechanism of their formation. There are generally two schools of speculation each with its experimental support: (1) one that believes the skin is formed because of the evaporation step involved<sup>5–10</sup>, and (2) one that suggests that precipitation is the responsible cause.<sup>10–13</sup> Besides, Gittens et al.<sup>8,9</sup> have detected, by electron microscopy, a three-layer structure consisting of an upper “active layer,” a “sub-layer,” and a “porous layer.” The thickness of each layer depends on evaporation conditions.

In this article, the application of scanning electron microscopy and transmission electron microscopy to such representative membrane problems as swelling, asymmetry, void size, pore size, and the morphological changes attendant upon acetone evaporation are considered. In addition, the membranes are

characterized in terms of thickness, water content, and free (freezing) and bound (nonfreezing) water. The effects of membrane preparation technique on morphology are also correlated with desalination properties.

## EXPERIMENTAL

### Membrane Preparation and Performance

The membranes were produced at  $1.5 \pm 0.2^\circ\text{C}$  in an atmosphere of a given humidity (88%) from casting solution consisting of 22.2 g cellulose diacetate (Eastman Kodak E 398-3), 66.7 g acetone, 9.99 g water, and occasionally 1.11 g of an anhydrous inorganic salt. Two types of salt were used: (1) swelling agents [ $\text{KSCN}$ ,  $\text{Mg}(\text{ClO}_4)_2$ ], and (2) gelling agent [ $\text{Al}(\text{NO}_3)_3$ ]. The thin films (0.15 mm) were produced on a laboratory casting machine which permitted complete control of the casting speed and evaporation time before immersion in an ice-water bath. By determining membrane performance as a function of casting speed, the optimum conditions were found and the casting speed was fixed at 10.5 ft/min. Membranes were generally examined in the "as cast" condition, i.e., without heat treatment. Some studies were made of membranes heat treated by immersion in a thermostatically controlled water bath at  $87^\circ\text{C}$ .

Thickness measurements were made with a sensitive micrometer from which readings could be estimated to  $1 \mu\text{m}$ . At least three repeat measurements were made at three different points, and the results were averaged.

The membranes were tested for salt rejection and volume flux in a stirred cell at 55 or 60 atm with a 0.5% aqueous solution of NaCl.

### Determination of Equilibrium Phase Separation Data

For the purpose of this determination the casting solution was treated as a ternary system consisting of polymer (cellulose diacetate), solvent (acetone), and nonsolvent (water or aqueous solution of inorganic salt).

At polymer concentrations of 15 wt % or less, the method used was essentially that described by Kunst and Sourirajan.<sup>5</sup> Stock solutions of different concentrations of CA in acetone [ $\sim 1.5$ , 5, 10, and 15 wt % polymer] were prepared and a thorough mixing was accomplished. After polymer was completely dissolved, several samples of each one of these stock solutions were weighed in glass-stoppered flasks. To each one of these flasks a calculated quantity of nonsolvent was added. After thorough mixing for one to several days at low values of nonsolvent-acetone ratio, mixtures gave clear solutions. At higher nonsolvent-acetone ratio, mixtures become more and more turbid because of polymer precipitation. The ternary system, the composition of which corresponded to the highest nonsolvent-acetone ratio yielding a clear solution, was then selected. Increasing amounts of nonsolvent were added to aliquots of this polymer solution. Sufficient time with intermittent shaking was allowed for the mixtures to reach phase equilibrium and constant turbidity.

The turbidity of the mixture was measured with a Cary 15 spectrophotometer. The wavelength used was 500 nm,<sup>1</sup> and the incipient cloud point was determined according to the method developed by Hong and Burns.<sup>14</sup> In this method, the concentration at the intersection of the two straight lines obtained by plotting the logarithm of the percent transmittance against polymer concentration was

interpreted as the incipient cloud point. Under these conditions, the boundary composition corresponding to the phase separation of the polymer was located within 0.5–1.5% of the total solution weight.

At polymer concentration higher than 15 wt %, the data were obtained following the method described earlier.<sup>3</sup> The turbidity caused by phase separation was recognized by visual observation, and the indicated locations of the boundary lines are less precise.

Tie lines were either taken from the work of Strathmann et al.<sup>11</sup> or determined according to the method developed by these authors. The critical point C was obtained by extrapolating the middle of the tie lines.

The sol–gel transition was achieved by controlled evaporation of acetone from 25 wt % CA solutions. The water content ranged from 0 to 15 wt %. The gelation of such solutions is first made evident by an increase in the viscosity. As acetone evaporation proceeds, the viscosity continues to rise and solutions become progressively less fluid. As the solutions gel, the viscosity becomes essentially infinite and the flow ceases.

### Total Water Content

A membrane sample of ~0.1–0.2 g equilibrated in the water bath was quickly blotted by a paper towel to remove surface water, then equilibrated with water vapors at 88% relative humidity and weighed. The membrane sample was then dried at 75°C under vacuum (0.01 torr) for sufficient time and weighed again. Water contents determined by the weight difference of the wet and dry samples were reproducible within  $\pm 2\%$ .

### Freezing and Nonfreezing Water Amounts

The amounts of free water (freezing) and bound water (nonfreezing) were determined according to previously described procedures.<sup>15,16</sup>

The samples studied by DSC were prepared at 2°C in an atmosphere of given humidity (88%) by drying the surfaces of the wet membrane with two damp filter papers and immediately packing the film as tightly as possible in aluminum pans which were sealed to prevent evaporation during the measurement. The sealed pans were cooled to  $-40^{\circ}\text{C}$  and then heated to  $+50^{\circ}\text{C}$ . The instrument used was a du Pont model 900 differential thermal analyzer operating at a heating rate of  $10^{\circ}\text{C}/\text{min}$ .

The area under the melting peak curve was measured and the amount of freezing water computed from a calibration curve obtained from weighed samples of pure water. Typical melting endotherms of pure water and water in membranes are shown in Figure 1. The areas of the melting peaks given in this figure were reproducible to 3% on repeated runs. Comparing the shapes of the melting peaks shown in Figure 1, one notices that (1) the melting endotherms of water in membranes start at  $10\text{--}15^{\circ}\text{C}$  lower than the melting peak of pure water, and (2) they consist of a sharp and a broad component. These results are very similar to those obtained by Taniguchi and Horigome<sup>17</sup> for membranes prepared from casting solution consisting of 25 g CA–45 g acetone and 30 g formamide and by Burghoff and Pusch<sup>18</sup> for membranes cast from chloroform solutions of CA. The sharp component can be related to the completely free water, and the broad one, to the free water interacting very weakly with polymer chains.

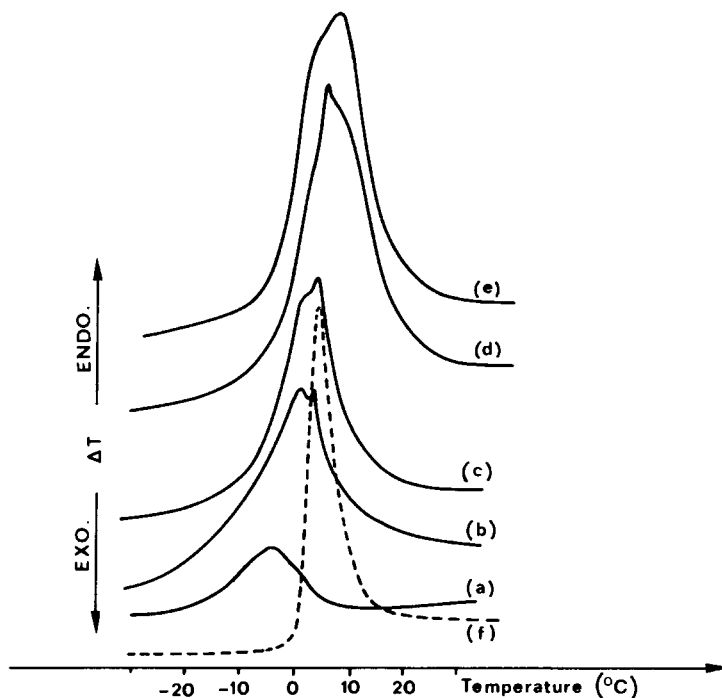


Fig. 1. Typical DSC melting endotherms of water in  $\text{Mg}(\text{ClO}_4)_2$ -cast membranes and of pure water: (a) 29.6%; (b) 31%; (c) 42.1%; (d) 54.7%; (e) 65.5%; (f) pure water.

The amount of nonfreezing water was taken as the difference between the total water content and the amount of freezing water.

### Scanning Electron Microscopy

For the scanning electron micrographs of membrane cross sections, samples were prepared by fracturing the membranes at liquid nitrogen temperature, lyophilizing, and coating with gold.

### Transmission Electron Microscopy

The samples were prepared in an atmosphere of given humidity (88%) by drying the surface of the wet membrane with damp filter papers and trimming the film to the proper size to fit in a sample holder. The sample holder and the sample were immersed immediately in liquid Freon 22 at  $-160^\circ\text{C}$  to freeze the membrane without causing large crystals of ice which would disrupt the membrane structure.

The tiny ice crystals produced were sublimed from the specimen at  $-100^\circ\text{C}$  into a vacuum of  $10^{-4}$  torr. The frozen membrane was then cross-sectioned using a Balzers ultramicrotome. A knife temperature of  $-170^\circ\text{C}$  and a specimen temperature of  $-100^\circ\text{C}$  were optimum. The cross sections obtained were shadowed with evaporated platinum-carbon, after which they were coated with a layer of evaporated carbon. They were allowed to float at room temperature on distilled water overnight and picked up onto microscope grids. The cellulose

diacetate was then dissolved using pure acetone, and the replicas were observed in the transmission microscope.

## RESULTS

In a previous article<sup>3</sup> we have studied the kinetics of acetone evaporation from films obtained by casting solutions of CA–acetone–water–inorganic salt. Three successive regimes of evaporation have been identified. The first two are exponential and end, respectively, at critical times  $t_1$  and  $t_2$ . It was established that at time  $t_1$  a modification occurs at the film surface, giving rise to a layer with a different structure and that  $t_2$  corresponds to the complete gelation of the medium. In order to help readers better understand the discussion, a typical evaporation curve is shown in Figure 2 and the values of  $t_1$  and  $t_2$  times are reported in Tables I–III. Gelling agents added to the casting solution were found to be effective in decreasing both  $t_1$  and  $t_2$ . The opposite effect was observed with swelling agents. As the rate of loss of acetone was found independent of the nature of the additive, such effects have to be assigned to changes in the concentration of water required for initiating phase separation.

The composition at which phase separation occurs with respect to the specified polymer (CA)–solvent (acetone)–nonsolvent (water with eventually an inorganic salt) systems are plotted in a triangular diagram in Figure 3, where the point I represents the composition of the casting solution used in making membranes for this study. For the CA–acetone–aqueous magnesium perchlorate system, our results are in good agreement with the phase boundary curve reported earlier by Kunst and Sourirajan.<sup>5</sup> As shown in our previous article,<sup>1</sup> the stronger the swelling salt, the greater the amount of water at the phase boundary.

During acetone evaporation, the average composition of the cast solution will change along the line IE. At  $t_1$  sec after casting, the film surface composition path will touch the boundary curve at compositions corresponding to points a, o, k, and m for casting solutions containing  $\text{Al}(\text{NO}_3)_3$ , no additive, KSCN, and  $\text{Mg}(\text{ClO}_4)_2$ , respectively. Note that in solutions of CA, when the polymer concentration is high, many links between different polymer molecules are formed and the system can undergo a sol–gel transition.<sup>19–21</sup> Thus, as shown in Figure 3 for KSCN or  $\text{Mg}(\text{ClO}_4)_2$  systems, at time  $t_1$  the evaporation-formed layer at the air–casting solution interface can be regarded as a solid (gel). As pointed out by Strathmann et al.,<sup>22</sup> further bulk movement of the polymer is hindered. As evaporation proceeds, more solvent is lost and the solidified layer thickens. At evaporation time  $t_2$ , it extends the full thickness of the film. Figure 3 indicates that the solidification of the film will be complete at compositions corresponding to points a', o', k', and m' for casting solutions containing  $\text{Al}(\text{NO}_3)_3$ , no additive, KSCN, and  $\text{Mg}(\text{ClO}_4)_2$ , respectively. An evaporation time higher than 480 sec is generally required to obtain the composition corresponding to the point E.

Phase inversion can be also achieved by immersing the cast film into a precipitation bath of ice water either directly or after a predetermined evaporation period. As illustrated in Figure 3 for systems containing  $\text{Mg}(\text{ClO}_4)_2$ , the average precipitation pathway of casting solution during membrane formation is  $\text{IC}_0$ ,  $\text{ImC}_1$ , or  $\text{Im}'\text{C}_2$ , depending upon whether the evaporation time is 2 sec,  $t_1$ , or  $t_2$ . Composition at the immersion time, for example, compositions corresponding

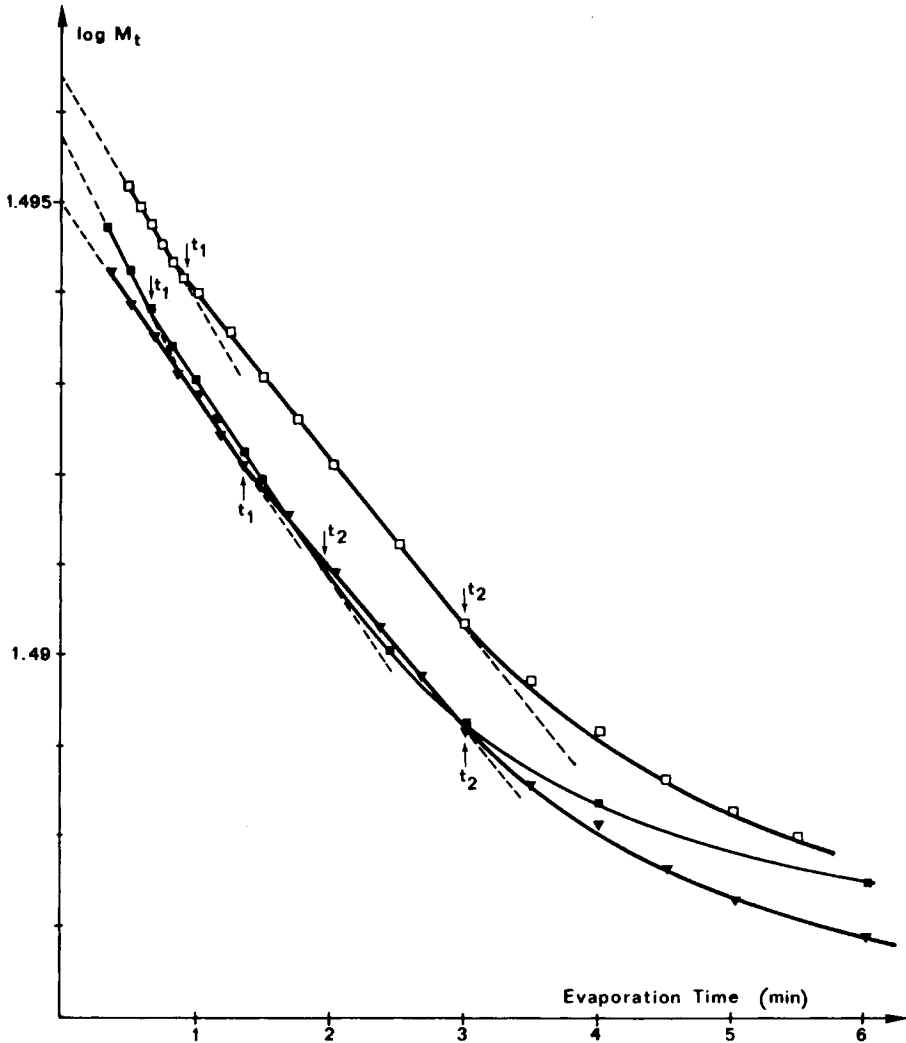


Fig. 2. Typical curve of acetone evaporation. Temperature 1.5°C. Casting solution composition: CA, 22.20 g; acetone, 66.70 g; water, 9.99 g; inorganic salt, 1.11 g.  $M_t$  is the weight of the casting plate plus film at any time  $t$ : ( $\blacktriangledown$ )  $\text{Mg}(\text{ClO}_4)_2$ , ( $\square$ ) KSCN; ( $\blacksquare$ )  $\text{Al}(\text{NO}_3)_3$ .

to points  $m$  and  $m'$  can be determined from the plot of Figure 2 which connects the acetone loss to evaporation time. The positions  $C_0$ ,  $C_1$ , and  $C_2$  on line WP determine the overall porosity of the resultant membranes. As the period of evaporation increases, the point which represents the final membrane composition moves from point  $C_0$  to a point close to E.

A set of membranes was made using a casting solution composed of CA-acetone-water and inorganic salt 22.2:66.7:9.99:1.11 (or 0) represented by point I and increasing the evaporation period from 0 to 480 sec. Their performance data are given in Table I and Figures 4 and 5. With the exception of membranes cast from systems where there is no inorganic salt which are only slightly permeable to water, it is apparent that before heat treatment, a region of maximum water permeability and minimum salt-rejecting property is located between two

TABLE I  
Influence of Air Exposure Period prior to Leaching on Desalination Characteristics of Membranes Prepared from CA 22.2 g-Acetone 66.7 g-Water 9.99 g and eventually  $\text{Al}(\text{NO}_3)_3$  1.11 g Casting Solution<sup>a</sup>

Inorganic salt	Evaporation time, sec	As-cast membranes			Membranes heat treated at 86°C		
		Flux, $\text{l/m}^2\text{-day}$	Salt rejection, %	Remarks	Flux, $\text{l/m}^2\text{-day}$	Salt rejection, %	Remarks
$\text{Al}(\text{NO}_3)_3$	2	560	4	opaque	352	46	opaque
	6	590	6	opaque	370	44	opaque
	12	1170	18	opaque	228	11	opaque
	$t_1 = 40$ sec						
	60	20	21	opaque	10	44	opaque
	100	16	25	opaque			
	$t_2 = 120$ sec						
	150	12	29	opaque			
	240	8	10	opaque			
	Without salt	2	13	23	opaque		
6		13.5	23	opaque			
30		12	50	opaque			
$t_1 = 60$ sec							
90		16	68	opaque			
$t_2 = 120$ sec							
150		9	80	opaque			

<sup>a</sup> Operating pressure: 60 bars.

characteristic times. It is worthwhile to note that a correlation can be made between these evaporation times and the critical times  $t_1$  and  $t_2$ .

Electron micrographs of cross sections of "as cast" membranes (Figs. 6-8) reveal morphological differences which can be schematized, as shown in Figure 9, by considering four types of structure, each associated with characteristic membrane properties:

TABLE II  
Water Contents and Free and Bound Water Amounts of "As Cast" Membranes Prepared from Casting Solutions Containing  $\text{Mg}(\text{ClO}_4)_2$

Evaporation time, sec	Total water content in wet membrane, %	Free water content in wet membrane, %	Bound water content in wet membrane, %	Weight, g, of free water per g dry CA	Weight, g, of bound water per g dry CA	Remarks
2	65.5	46.1	19.4	1.34	0.56	slightly turbid
60	57.0	36.5	20.5	0.85	0.48	transparent
$t_1 = 80$ sec						
90	54.7	33.4	21.3	0.74	0.47	transparent
100	54.4	32.7	21.7	0.72	0.48	transparent
110	54.2	31.5	22.7	0.69	0.50	transparent
150	53.4	28.2	25.2	0.61	0.54	transparent
$t_2 = 180$ sec						
240	42.1	22.1	20.0	0.38	0.35	transparent
480	34.1	11.6	22.5	0.18	0.34	transparent
1500	31.0	9.8	21.2	0.14	0.31	transparent
2700	29.6	8.2	21.4	0.12	0.30	transparent

TABLE III  
Water Contents and Free and Bound Water Amounts of "As Cast" Membranes Prepared from Casting Solutions Containing KSCN

Evaporation time, sec	Total water content in wet membrane, %	Free water content in wet membrane, %	Bound water content in wet membrane, %	Weight, g, of free water per g dry CA	Weight, g, of bound water per g dry CA	Remarks
2	63.7	37.6	26.1	1.04	0.72	opaque
20	64.3	33.7	30.6	0.94	0.86	opaque
$t_1 = 60$ sec	61.6	28.4	33.2	0.74	0.87	turbid
90	61.7	35.9	25.8	0.94	0.67	slightly turbid
120	62.2	25.6	36.6	0.68	0.97	transparent
150	57.1	24.9	32.2	0.57	0.76	transparent
$t_2 = 180$ sec						
240	41.2	17.6	23.6	0.30	0.40	transparent
330	37.2	13.2	24.0	0.21	0.38	transparent
480	36.7	11.8	24.9	0.18	0.39	transparent

Structure A corresponds to the layer of KSCN or  $Mg(ClO_4)_2$  cast membranes which is formed prior to immersion in water as a consequence of acetone evaporation. Thus, while structure A appears only in the surface layer in the case of membranes obtained with an evaporation period barely longer than  $t_1$ , it extends the full thickness of membranes at evaporation times longer than  $t_2$ .

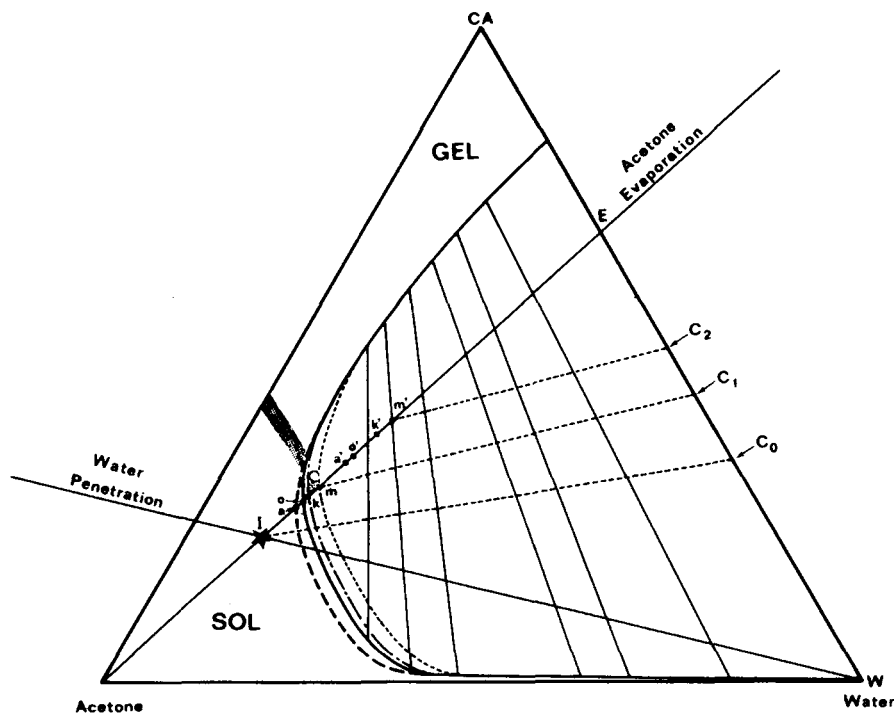


Fig. 3. Equilibrium phase separation compositions (wt %) for the ternary systems cellulose acetate-acetone-water and, eventually, inorganic salt: (---)  $Mg(ClO_4)_2$ ; (- - - -) KSCN; (—) saltless; (- - - -)  $Al(NO_3)_3$ .



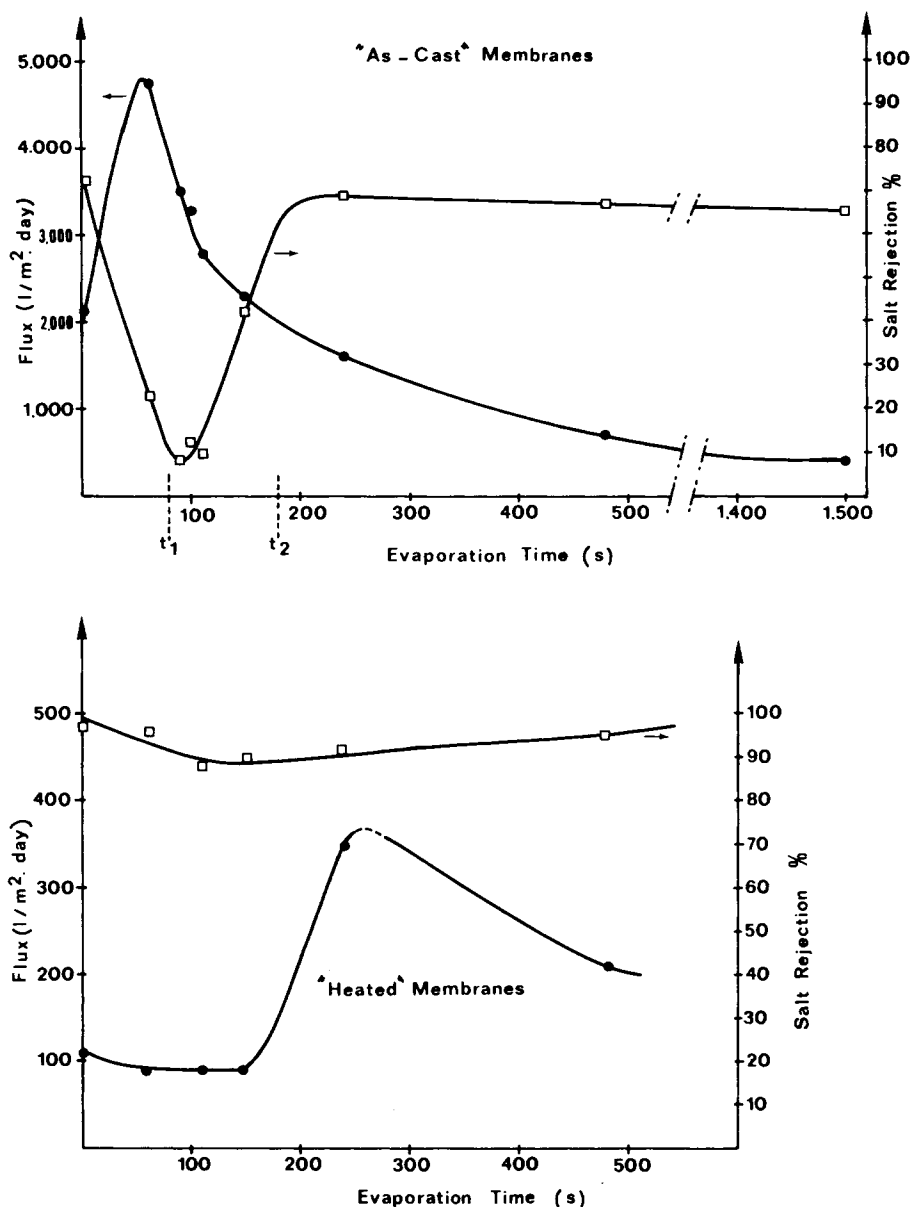


Fig. 4. Influence of air exposure period prior to leaching on the desalination characteristics of membranes prepared from CA 22.2 g-acetone 66.7 g-water 9.99 g- $\text{Mg}(\text{ClO}_4)_2$  1.11 g casting solution.

Electron micrographs of cross sections of type A membranes appear uniform and show no porosity whatsoever, even at a magnification of 40,000 $\times$  (Fig. 10).

Structure B is that of the upper layer, i.e., the air-casting solution interface, of membranes that were allowed to evaporate for a time shorter than  $t_1$ . It also forms partly or wholly the sublayer of membranes prepared from KSCN or  $\text{Mg}(\text{ClO}_4)_2$  systems with an evaporation period in the range of  $t_1$ - $t_2$ . This structure is very similar to structure A; and in the scanning electron micrograph

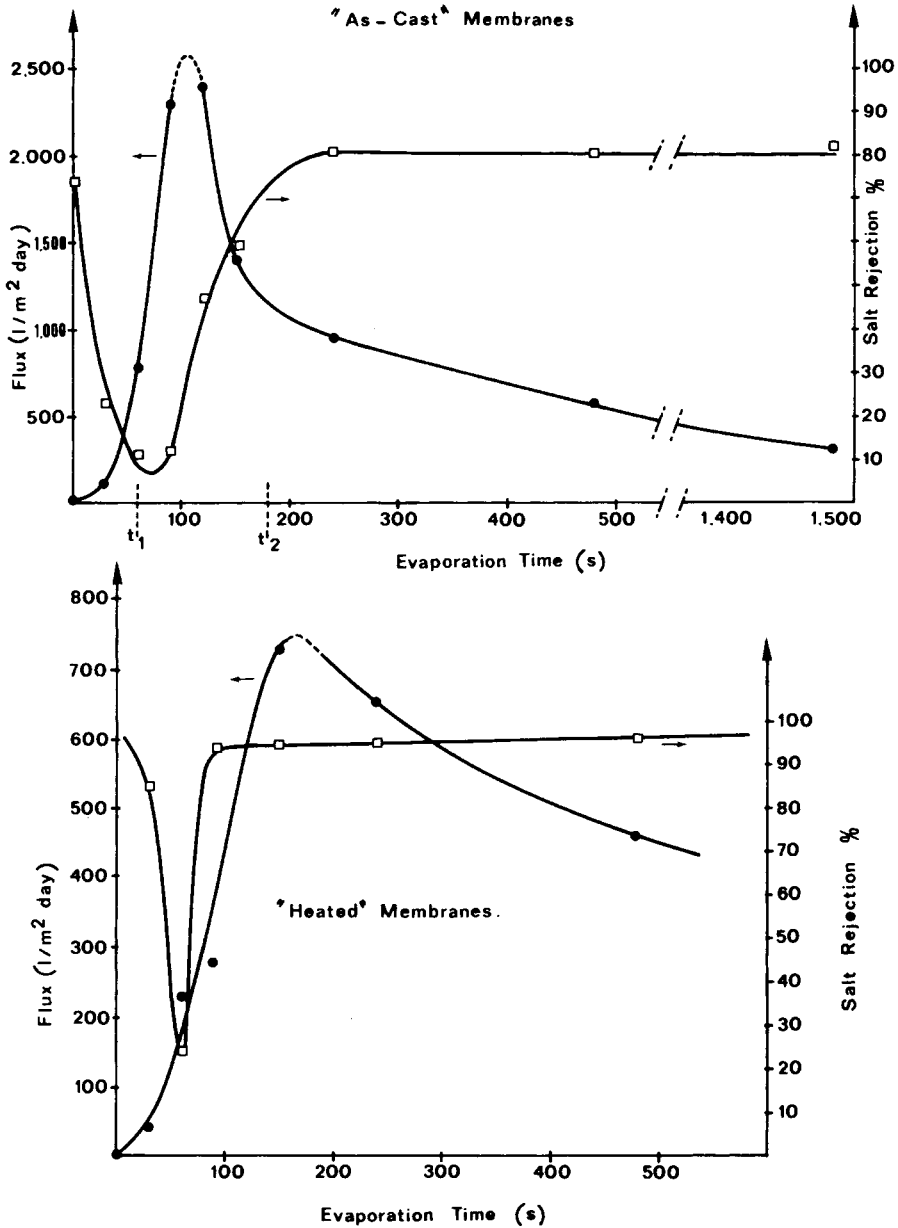


Fig. 5. Influence of air exposure period prior to leaching on the desalination characteristics of membranes prepared from CA 22.2 g-acetone 66.7 g-water 9.99 g-KSCN 1.11 g casting solution.

of cross sections of KSCN- or  $Mg(ClO_4)_2$ -cast membranes [Figs. 8(d) and 8(e)], the boundary between A and B layers is poorly defined, although there are clearly visible differences in texture which were reproducible. Only higher magnification transmission electron micrographs show that structure B is less dense than structure A.

Structure C is an open network of pores with some interpore connections and

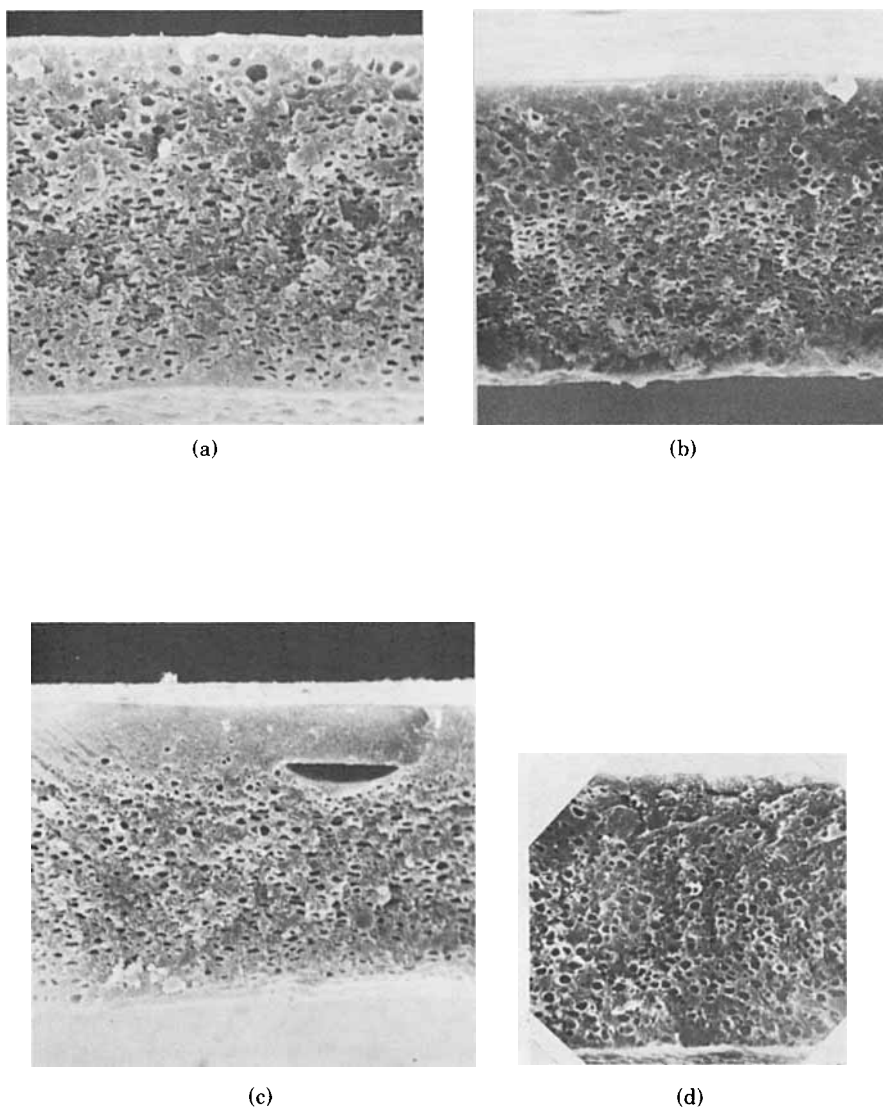


Fig. 6. Scanning electron micrographs of cross sections of CA membranes cast from solutions where there is no inorganic salt and dried 0 sec (a), 30 sec (b), 90 sec (c), and 150 sec (d) prior to their immersion ( $G = 2000$ ). (The upper region of the cross sections corresponds to the air-casting solution interface.)

very thin CA walls (Fig. 11). The high pore density remains practically constant throughout the C layer. The pore diameter in the direction perpendicular to the membrane surface is larger than that in the parallel direction. The size of pores tends to increase from the B-C junction to the back edge of the membrane. Besides, the pore size in KSCN-cast membranes is smaller than that in  $\text{Al}(\text{NO}_3)_3$ -cast membranes. There is also a gradual decrease in pore volume as evaporation time increases until structure C contains no large pores.

Structure D (Fig. 11) is a closed pore structure. It features numerous pores of large size surrounded by areas of membrane matrix. The thickness of the CA inter-pore walls is large compared with that in the C structure. The pore size

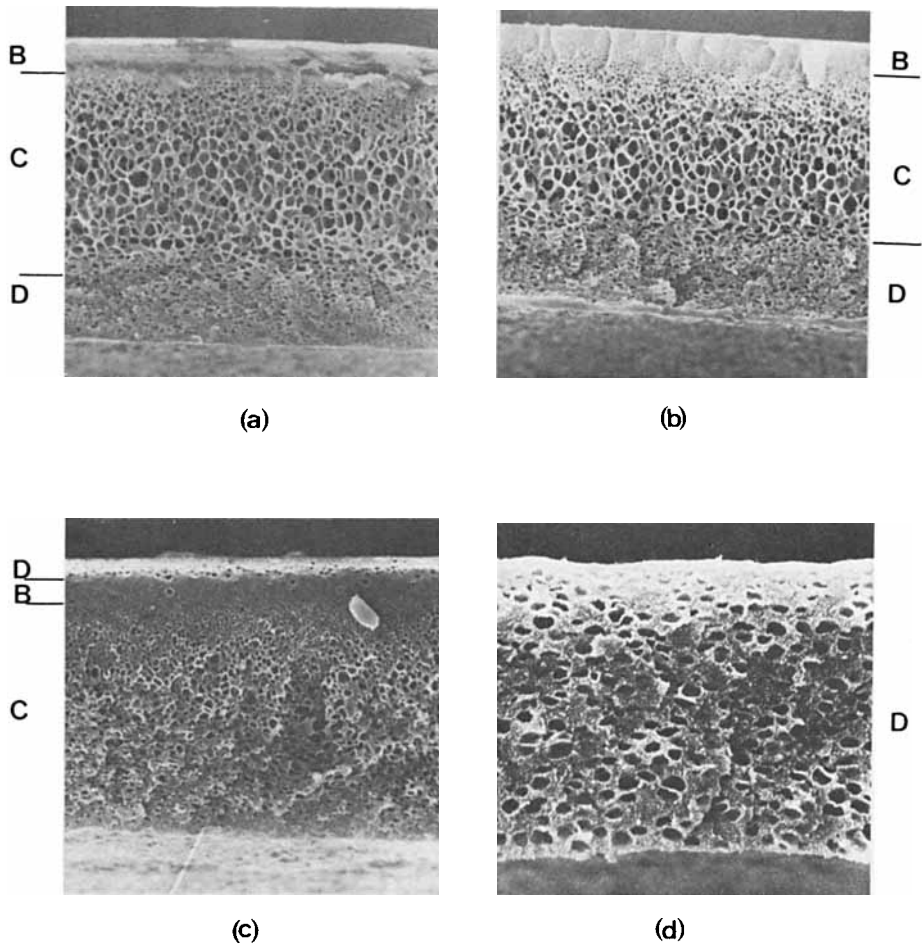


Fig. 7. Scanning electron micrographs of cross sections of CA membranes cast from solutions containing  $\text{Al}(\text{NO}_3)_3$  and dried 0 sec (a), 12 sec (b), 60 sec (c), and 150 sec (d) prior to their immersion ( $G = 2000$ ). (The upper region of the cross sections corresponds to the air-casting solution interface.)

remains fairly constant at about  $0.4 \mu\text{m}$  diameter. In fact, one notices a flattening of pores into oblate spheroids in the direction parallel to the membrane surface. Such a structure is the typical one of membranes prepared from casting solution where there is no inorganic salt (Fig. 6). Very often, as observed by Gittens et al.,<sup>8</sup> C and D structures occur together in the same membrane [Fig. 8(a)]. The D structure, immediately below layer C, appears near the back edge of the membrane.

Examination of Figure 9 suggests that structures A and B are associated with a high water permeability, this being particularly apparent in the case of the KSCN-containing system whose water flux increases as a consequence of the growth of the B structure at the expense of structures C and D as the evaporation time increases from 0 to 110 sec. On the other hand, structure D appears to be impermeable. For example, the comparison of performance and electron micrographs of cross sections of  $\text{Al}(\text{NO}_3)_3$ -cast membranes provides evidence that

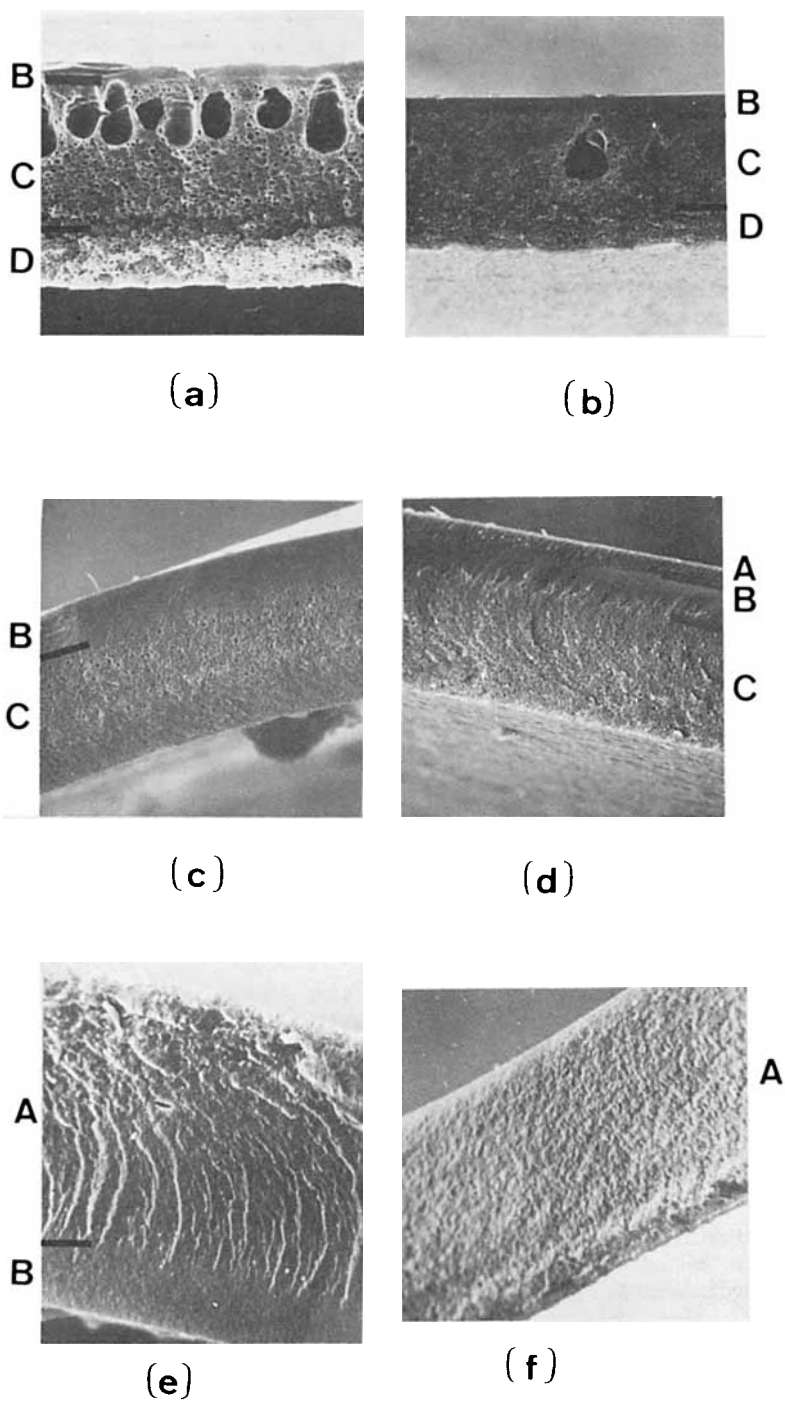











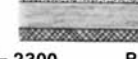

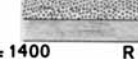




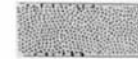



Fig. 8. Scanning electron micrographs of cross sections of CA membranes cast from solutions containing KSCN and dried 0 sec (a), 30 sec (b), 60 sec (c), 90 sec (d), 170 sec (e), 240 sec (f). (Lines denote upper layer/sublayer and sublayer/lower layer interfaces.)

Al (NO <sub>3</sub> ) <sub>3</sub>	no additive	K S CN	Mg (ClO <sub>4</sub> ) <sub>2</sub>
t = 0-2s  F = 560    R = 4 F <sub>H</sub> = 352    R <sub>H</sub> = 46	t = 0-2s  F = 13    R = 23	t = 0-2s  F = 30    R = 74	t = 0-2s  F = 2130    R = 73 F <sub>H</sub> = 110    R <sub>H</sub> = 97
t = 12s  F = 1170    R = 18 F <sub>H</sub> = 228    R <sub>H</sub> = 11 t <sub>1</sub> = 40s	t = 30s  F = 12    R = 50 60s	t = 30s  F = 130    R = 23 F <sub>H</sub> = 40    R <sub>H</sub> = 85 60s	t = 60s  F = 4750    R = 23 F <sub>H</sub> = 85    R <sub>H</sub> = 96 80s
t = 60s  F = 20    R = 21 F <sub>H</sub> = 10    R <sub>H</sub> = 44	t = 90s  F = 16    R = 68 t = 110s  F = 17    R = 74 120s	t = 90s  F = 2300    R = 12 F <sub>H</sub> = 280    R <sub>H</sub> = 94 t = 110s  t = 150s  F = 1400    R = 59 F <sub>H</sub> = 730    R <sub>H</sub> = 95 180s	t = 110s  F = 2810    R = 10 F <sub>H</sub> = 95    R <sub>H</sub> = 88 t = 150s  F = 2300    R = 48 F <sub>H</sub> = 90    R <sub>H</sub> = 90 180s
t <sub>2</sub> = 120s t = 150s  F = 12    R = 29	t = 150s  F = 9    R = 80	t = 240s  F = 950    R = 81 F <sub>H</sub> = 650    R <sub>H</sub> = 95	t = 240s  F = 1600    R = 69 F <sub>H</sub> = 350    R <sub>H</sub> = 92

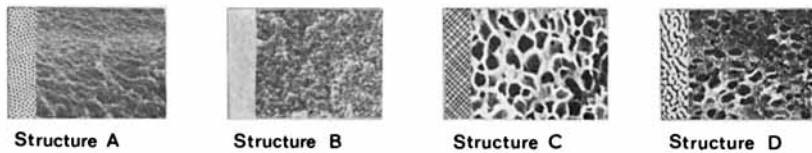


Fig. 9. Schematic representation of membrane structure. *F*: Flux (l/m<sup>2</sup>-day) of "as cast" membranes; *R*: salt rejection (%) of "as cast" membranes; *F<sub>H</sub>* and *R<sub>H</sub>*: desalination characteristics of heat-treated membranes.

the development of structure D causes a sharp decrease in water flux. Such an effect may be attributed to the rigid nature of the membrane matrix in this type of structure, owing to the great thickness and density of the interpore walls. In fact, transport coefficient measurements<sup>23</sup> have shown that the specific hydraulic permeability of the different structures increases in the order

$$D \text{ type} \ll C \text{ type}, A \text{ type} \ll B \text{ type}$$

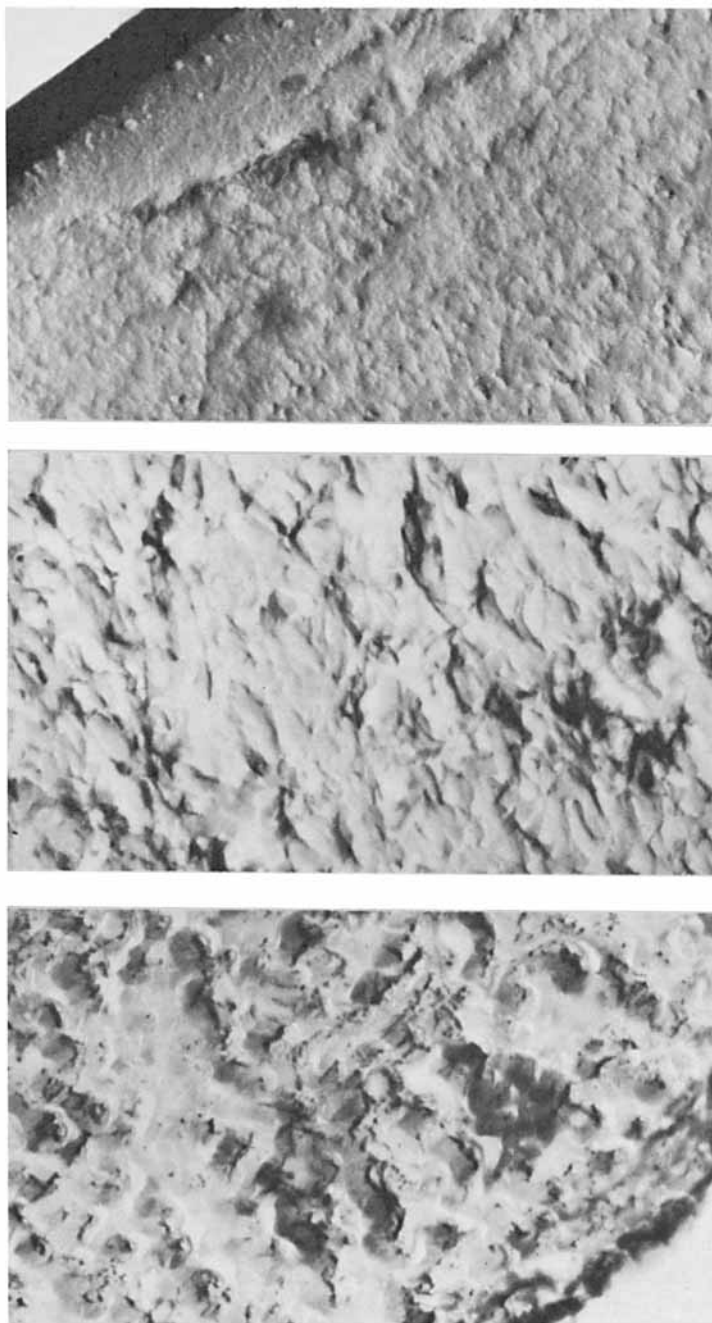
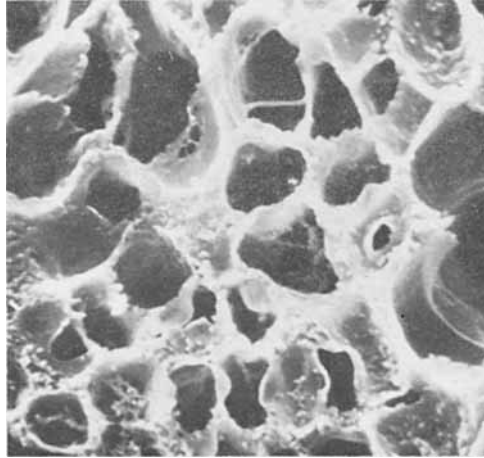


Fig. 10. Transmission micrograph of a 4-min evaporation time  $\text{Mg}(\text{ClO}_4)_2$  membrane showing a typical A structure (40,000 $\times$ ).

Finally, some voids exist in the  $\text{KSCN}$ - or  $\text{Mg}(\text{ClO}_4)_2$ -cast membranes obtained by short evaporation. In accordance with the observations made by Gittens et al.,<sup>9</sup> these large voids are closed and appear below the upper layer of presumably B structure, as shown, in scanning and transmission electron micrographs [Figs. 8(a), 8(b), and 12].



(a)



(b)

Fig. 11. Scanning electron micrographs of the typical C-type structure (a) and D-type structure (b). Magnification 6000X.

The formation of fingerlike cavities growing in the fluid layer is generally associated with a high rate of polymer precipitation<sup>10,22,24,25</sup> and/or a low polymer solution viscosity.<sup>25-27</sup> Helmcke<sup>28</sup> suggested that such voids represent emptied pockets of desolvation liquid. Matz<sup>26</sup> related these fingerlike formations "to several effects noted in the literature for analogous systems and which derive from hydrodynamic instabilities connected with surface tension or viscosity changes." According to Strahtmann et al.,<sup>22</sup> as the result of syneresis, shrinkage stress in the solidified polymer cannot be relieved by creep relaxation of the polymer and the homogeneous skin layer ruptures. Once a finger has been initiated by rupture of the surface layer of polymer, shrinkage of the polymer matrix causes it to propagate by draining the freshly precipitated polymer, at the bottom of the finger, to the side of the finger. Another explanation was proposed by Frommer et al.<sup>27</sup> who suggested that the formation of large fingerlike cavities



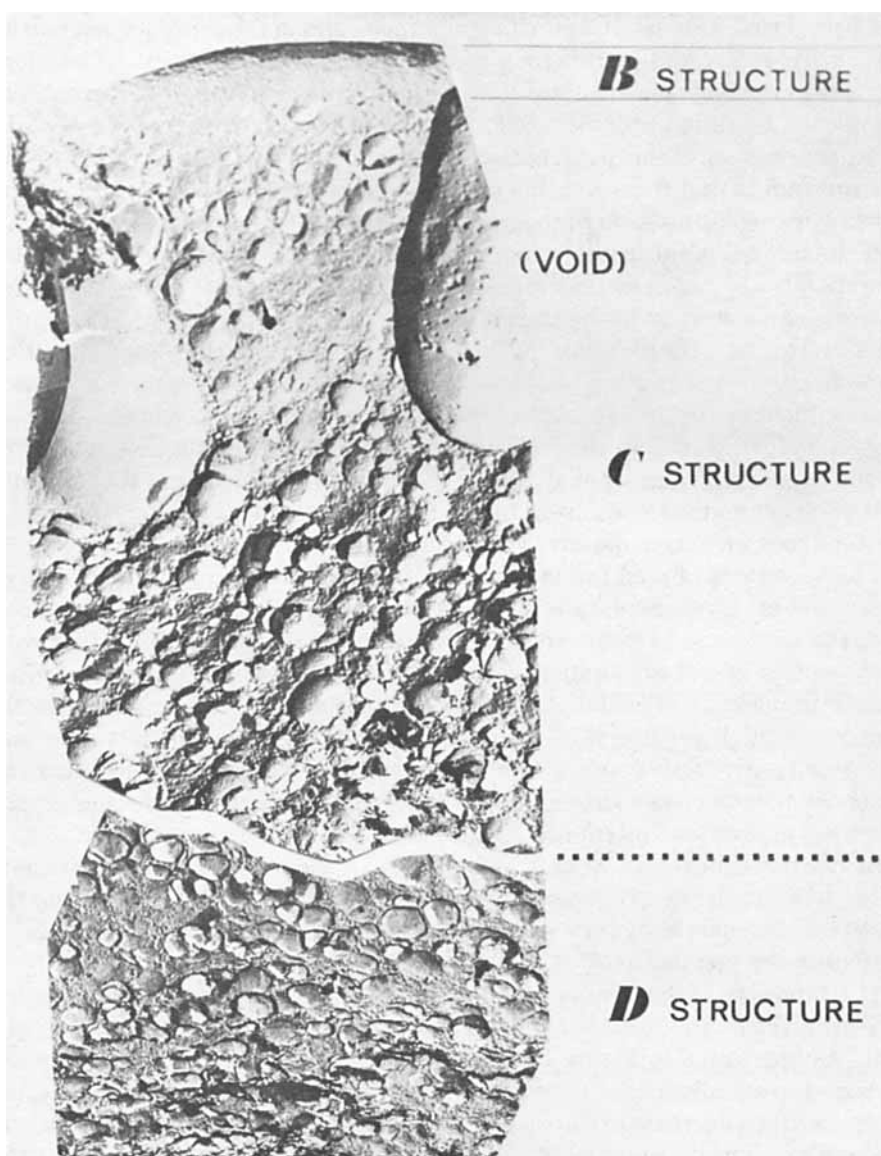


Fig. 12. Transmission micrograph of a 2-sec evaporation time KSCN membrane (5600 $\times$ ).

originates from convective flows formed within the cast (fluid) polymer solution upon its immersion in the bath of nonsolvent. The formation of these convective flows is associated with a high tendency of the nonsolvent and of the solvent to dissolve mutually in each other. Grobe et al.<sup>29</sup> suggested that the mass transfer is favored in places of the polymer-poor phase, the number of which is given by statistical distribution. The phase separation front will move faster in these places as a consequence of the faster exchange of solvent and nonsolvent. Because there is nonsolvent present in the polymer-poor dilute phase, solvent can reduce its chemical potential by diffusing into it. Eventually, the cavity will contain so much of the solvent that the coagulation at the boundary of the cavity

will be reduced. Solvation of the polymer molecules in the solution, just outside the cavity, is lowered by diffusion of the solvent into the cavity. Therefore, transfer of the polymer will occur to surrounding places by creep, and eventually complete desolvation will take place. In agreement with the recent observations of Koehnen et al.<sup>30</sup> this explanation seems the most probable. It allows the understanding that the formation of the fingerlike cavities is associated with a low polymer concentration in the casting solution.<sup>22,26,27,31</sup> Indeed, the tie lines and the critical point in the ternary phase diagram (Fig. 3) are such that the overall ratio of polymer-poor phase to polymer-rich phase increases as the polymer concentration in the casting solution decreases (i.e., as the evaporation time decreases). Besides, this model is in agreement with the observation that these fingerlike cavities can penetrate the solution further than the coagulation front without causing coagulation of the casting solution bypassed between these fingers.<sup>26,27,29</sup> Moreover, the explanation of Grobe et al.<sup>29</sup> is supported strongly by the results of Frommer et al.,<sup>10,24,27</sup> who found that the higher the tendency of the solvent and the nonsolvent to dissolve mutually in each other, the greater the tendency for fingerlike cavity formation.

The variations of membrane thickness and total water content with evaporation time are given graphically in Figures 13 and 14, respectively. All the curves have the same general form and can be divided into four parts: (1) a first part, in the early stages of evaporation, corresponding to a rapid and uniform decrease in membrane thickness and total water content; (2) a second part where the membrane thickness and total water content remain approximately constant; (3) a third part, corresponding to a transition zone, wherein the thickness and water content decrease sharply; and (4) a fourth part where the membrane thickness and water content are virtually independent of evaporation.

As discussed in ref. 23, such a dependence of the membrane thickness and water content on the evaporation time can be interpreted by considering the relative extent and the hydration characteristics of the different types of structure present in the membrane.

The variations of the freezing and nonfreezing water amounts with evaporation time are given in Tables II-V. The same behavior is observed for each inorganic salt. As illustrated in Figure 15, the weight of free water per gram of dry CA decreases gradually as the evaporation time increases, whereas there is some evidence that a decrease in the weight of bound water per gram of dry CA occurs at about  $t_2$ . The dependence of the weight of bound water per gram of dry CA on the evaporation time and the nature of the inorganic salt can be explained by a reasoning similar to that developed by Frommer et al.<sup>16</sup> The higher the density of the polymeric matrix of the membrane, the smaller the number of sites on a cellulosic chain which are not bound to another polymeric chain and are free to interact with water. For example, in the early stages of evaporation, the significantly lower total water content of the  $\text{Mg}(\text{ClO}_4)_2$ -cast membranes indicates that the density of the polymeric phase in these membranes is much higher than that of the KSCN-cast membranes. The weight of nonfreezing water per gram of dry CA is therefore only 0.47–0.56 g in the  $\text{Mg}(\text{ClO}_4)_2$ -cast membranes with an evaporation period shorter than 180 sec as compared to 0.67–0.87 g in the KSCN-cast membranes prepared under the same conditions.

On the contrary, beyond  $t_2$  the scanning and transmission electron micrographs show that the KSCN and  $\text{Mg}(\text{ClO}_4)_2$  membranes tend to have the same uniform

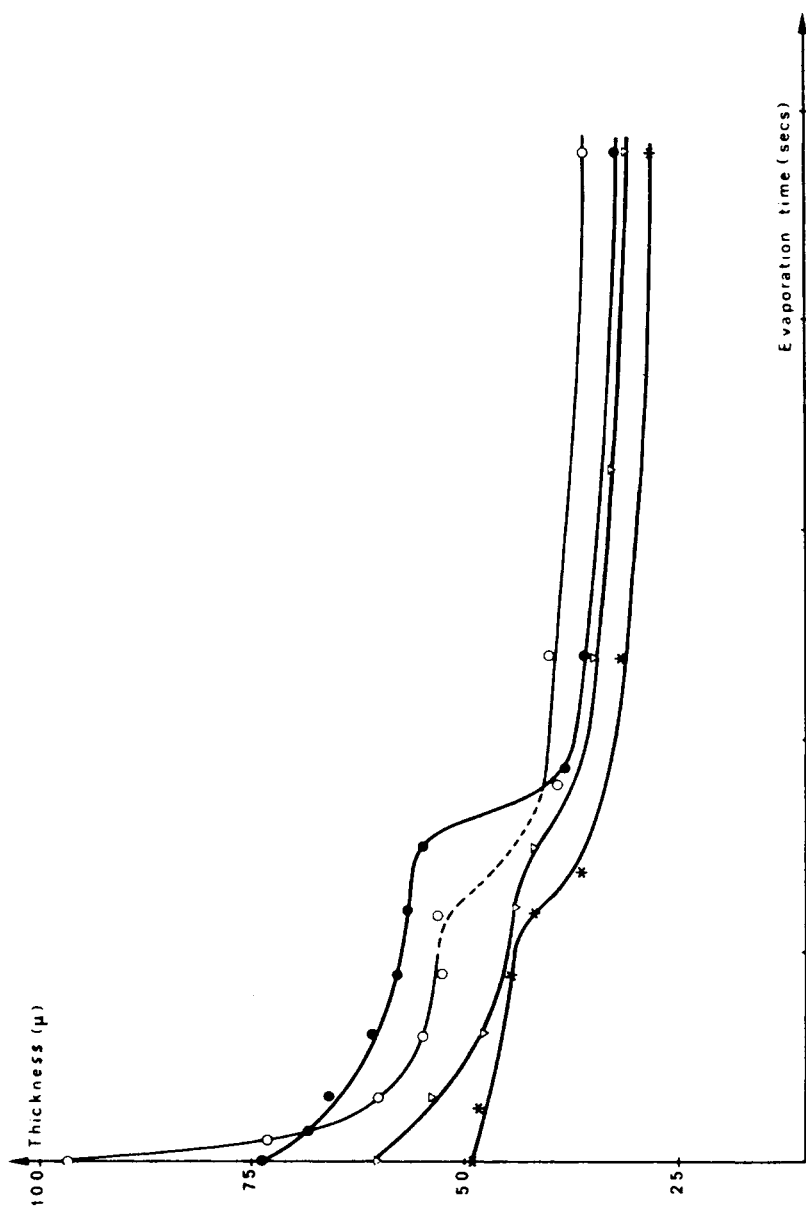


Fig. 13. Variations of membrane thickness with evaporation time for "as cast" membranes prepared from casting solutions where there is no inorganic salt or where the additive is  $\text{Al}(\text{NO}_3)_3$ ,  $\text{KSCN}$ , or  $\text{Mg}(\text{ClO}_4)_2$ : (●)  $\text{Mg}(\text{ClO}_4)_2$ ; (▽)  $\text{KSCN}$ ; (\*) saltless; (○)  $\text{Al}(\text{NO}_3)_3$ .

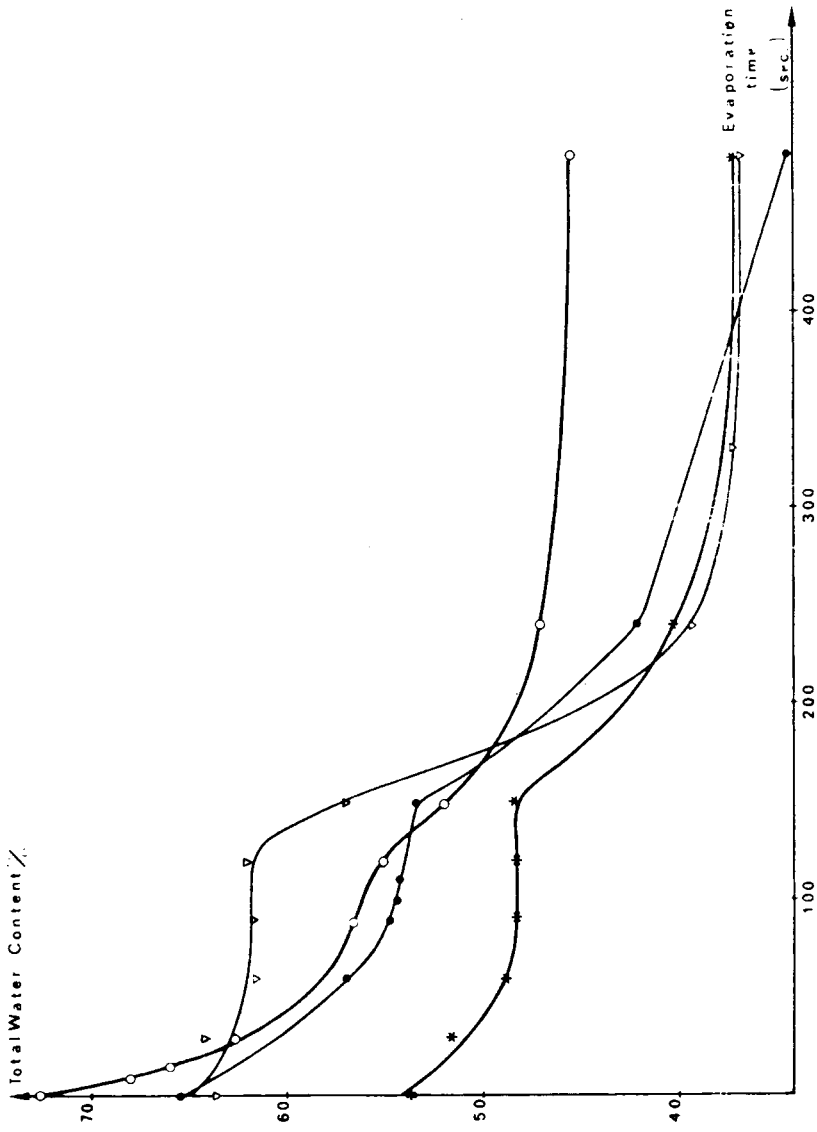


Fig. 14. Variations of water content with evaporation time for "as cast" membranes prepared from casting solutions containing  $\text{Mg}(\text{ClO}_4)_2$ ,  $\text{KSCN}$ ,  $\text{Al}(\text{NO}_3)_3$ , or no inorganic salt: (●)  $\text{Mg}(\text{ClO}_4)_2$ ; (▼)  $\text{KSCN}$ ; (○)  $\text{Al}(\text{NO}_3)_3$ ; (\*) saltless.

TABLE IV  
Water Contents and Free and Bound Water Amounts of "As Cast" Membranes Prepared from Casting Solutions Containing  $\text{Al}(\text{NO}_3)_3$

Evaporation time, sec	Total water content in wet membrane, %	Free water content in wet membrane, %	Bound water content in wet membrane, %	Weight, g, of free water per g dry CA	Weight, g, of bound water per g dry CA
2	72.7	54.8	17.9	2.01	0.65
9	68.1	50.1	18.0	1.57	0.56
15	66	48.2	17.8	1.42	0.52
30	62.8	42.8	20.0	1.15	0.54
$t_1 = 40$ sec					
90	56.9	35.8	21.1	0.83	0.49
$t_2 = 120$ sec	54.9	31.5	23.4	0.70	0.52
150	52.1	30.1	22	0.63	0.46
240	47.1	25.4	21.7	0.48	0.41
480	45.4	24.0	21.3	0.44	0.39

morphology. In addition, the total water content in the KSCN-cast membranes (240 sec, 41.2%; 480 sec, 36.7%) is very similar to that in the  $\text{Mg}(\text{ClO}_4)_2$ -cast ones (240 sec, 42.1%; 480 sec, 34.1%). We can therefore estimate that the packing density of the polymer within these membranes and, consequently, the extent of polymer-polymer interactions and the accessibility of the polymeric chains to interact with water are similar. The weight of nonfreezing water per gram of dry CA is therefore 0.4–0.39 g in the KSCN membranes as compared to 0.35–0.34 g in the  $\text{Mg}(\text{ClO}_4)_2$  membranes. In the same way, the more-or-less pronounced decrease in the weight of bound water per gram of dry CA can be related to the rapid increase in the thickness of the upper layer of the membranes which occurs at about  $t_2$ , as shown by electron micrographs and transport coefficient measurements.<sup>23</sup> Indeed, the surface layer is brought about by solvent evaporation prior to contact with water so that it exhibits a polymer packing density much higher than the other layers related to the quite distinct phenomenon of coagulation in water. As shown in the Discussion section of this article, membranes prepared from saltless solutions are mainly formed by diffusion of acetone from the solution into air or water, without the intervention of any water penetration. As a consequence, the bound water content remains practically the same whatever the evaporation period involved in the membrane making procedure may be.

TABLE V  
Water Contents and Free and Bound Water Amounts of "As Cast" Membranes Prepared from Casting Solutions Containing no Inorganic Salt

Evaporation time, sec	Total water content in wet membrane, %	Free water content in wet membrane, %	Bound water content in wet membrane, %	Weight, g, of free water per g dry CA	Weight, g, of bound water per g dry CA
2	53.5	39.1	14.4	0.84	0.31
30	51.5	34.5	17	0.71	0.35
$t_1 = 60$ sec					
90	48.4	30.4	18	0.59	0.35
$t_2 = 120$ sec	48.2	26.4	21.8	0.51	0.42
150	48.2	30.1	18.1	0.58	0.35
240	40.4	21.4	19.0	0.36	0.32
480	36.8	18.4	18.4	0.29	0.29

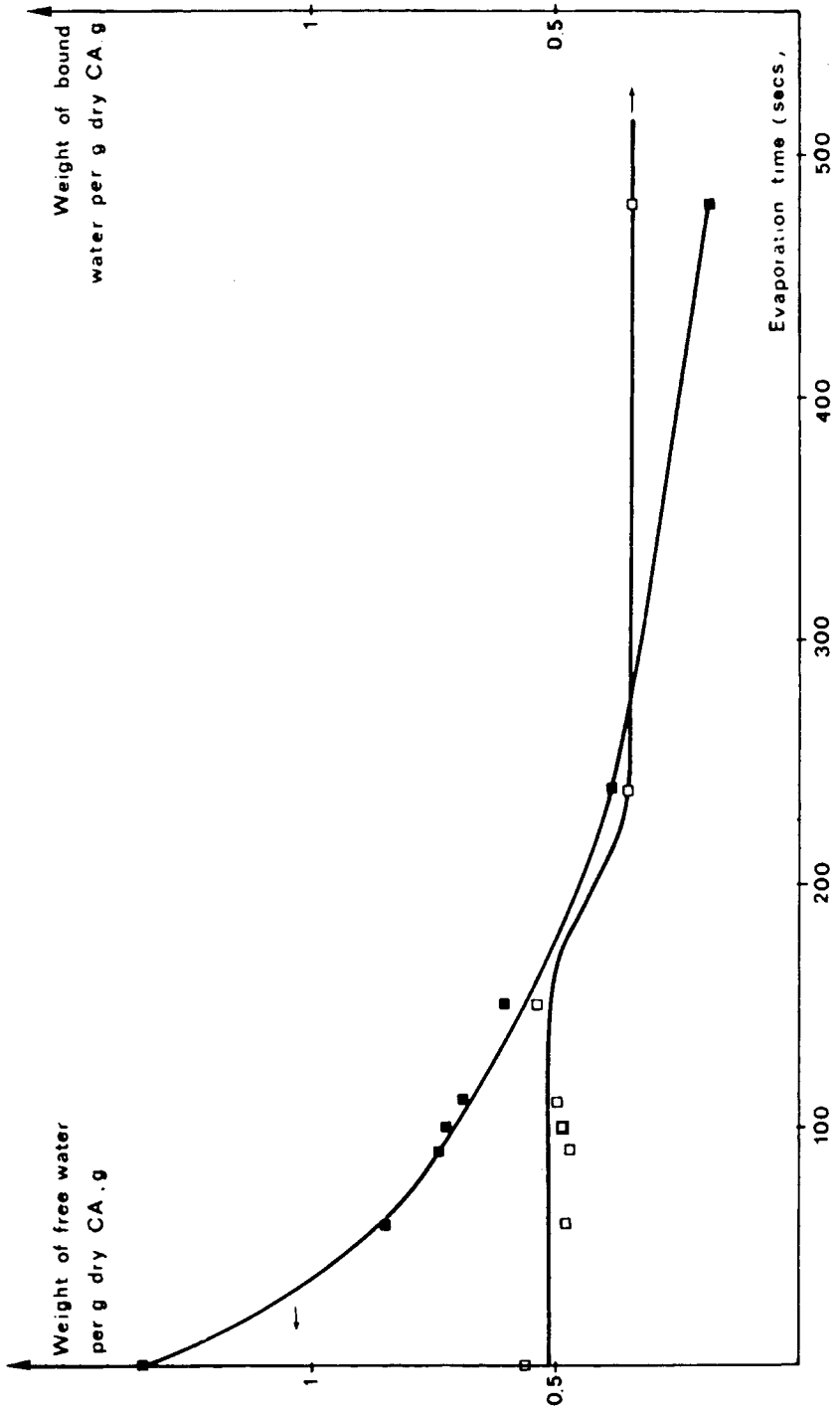


Fig. 15. Dependence of free water and bound water contents on evaporation time for "as cast" membranes prepared from casting solutions containing  $Mg(ClO_4)_2$ .

## DISCUSSION

## Effect of Inorganic Salt

Tables I–V and Figures 4–8, 13, and 14 show differences in the turbidity, thickness, hydration, structure, and performance of membranes that were cast from either saltless or salt-containing casting solutions and immersed in the water bath within 2 sec from their casting.

Since the preparation procedure was identical in the four cases, it is obvious that these differences must be attributed to the nature of the inorganic salt. The addition of an inorganic salt to casting solution is expected to modify the following parameters:

(1) The structure of the casting solution. Viscosity measurements allowed to establish the following sequence for the increase in viscosity of casting solutions as a function of the inorganic salt:

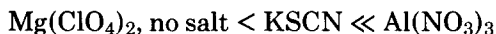
$$\begin{array}{ccccccc} \text{saltless} & < & \text{Al(NO}_3)_3 & < & \text{KSCN} & < & \text{Mg(ClO}_4)_2 \\ \eta_{25^\circ}, cp = 1632 & & 1790 & & 2006 & & 2272 \end{array}$$

(2) The phase diagram and, consequently, the composition at the phase boundary. The precipitation point was found<sup>1</sup> (Fig. 3) to depend on the type of salt contained in the solution. With  $\text{Al(NO}_3)_3$ , precipitation required less water than a saltless solution. With  $\text{Mg(ClO}_4)_2$ , more water was needed. KSCN had only a small effect on the precipitation point.

(3) The kinetics of acetone evaporation and the acetone concentration gradient within the cast film.<sup>3</sup>

(4) The rate of penetration of water into the immersed cast film and the acetone outflux. It has been shown by Frommer<sup>32</sup> and Strathmann<sup>11</sup> that the action of casting solution additives is to decrease the difference in the chemical potential of the acetone and to increase the difference in the chemical potential of the water between the casting solution and the wash bath. Thus, as pointed out by Kraus<sup>33</sup> and from our own experience, the rate of flow of acetone out of the cast film will be reduced relative to the rate of water flow into the polymer solution in the case of salt-containing casting solutions. The higher the number of particles in solution [ $\text{saltless} < \text{KSCN} < \text{Mg(ClO}_4)_2 < \text{Al(NO}_3)_3$ ], the more marked this effect.

Finally, the speed of membrane coagulation in the leaching bath increases in the order<sup>1</sup>



Referring to previous data<sup>2</sup> on preferential solvation of CA chains in casting solutions containing different inorganic salts, “gelling” agents were found to be effective in increasing attractive force between CA chains. It results in a more extensive supermolecular structuralization of the casting solution. The macromolecular chain average conformation is more coiled, and the dimensions of the supermolecular aggregates are larger than in saltless solutions. The resultant casting solution structure would be heterogeneous and might contain microgels. Besides, as is seen from Figure 3, with “gelling” agents such as  $\text{Al(NO}_3)_3$ , the casting solution composition approaches more closely the boundary of the solubility region. Therefore, decreasing amounts of water need to diffuse into the cast film to cause phase separation, and decreasing amounts of acetone would

be able to diffuse out before polymer precipitation sets in. Moreover, the rate of solvent outflow is greatly reduced relative to the rate of coagulant flow into the polymer solution. These phenomena and the relatively low viscosity of the casting solution result in high rates of desolvation and precipitation. The phase inversion process takes place within a solution, the polymer concentration of which is practically the same as that of the original solution (Fig. 3).

An explanation similar to that proposed by Koenhen et al.<sup>30</sup> for the formation of the spongelike structure in the system polyurethane–dimethylformamide–water evokes liquid–liquid phase separation. As illustrated in Figure 3, such a system passes the border of the two-phase region at the diluted side of the critical point C. Under these conditions, droplets of the concentrated phase are expected to be formed with a large difference in composition from the original solution. As precipitation proceeds, the diluted phase continuously tends to pure water while droplets grow until they touch each other and coalesce, getting more and more polymer concentrated. Thus, when precipitation has come to an end, the polymer concentration in the concentrated phase is high enough for the precipitated polymer to be regarded as a solid, and owing to coalescence or sticking of the polymer spheres, an open-pore structure “C” is obtained in which membrane structure did not collapse because of the loss of solvent.<sup>11,34,35</sup> Resultant membranes [cast from  $\text{Al}(\text{NO}_3)_3$  system and immediately leached] are thick (97  $\mu\text{m}$  as compared to the saltless membrane thickness of 50  $\mu\text{m}$ ), white, opaque, and swollen as indicated by their water content (72.7% in comparison with 53.5% for the saltless membrane). This is in accordance with the observation shown in Figure 7(a) that these membranes contain numerous pores larger than 0.5  $\mu\text{m}$ . Such membranes have a low or no tendency to reject salt but a significant water flux (Table I) before heat treatment. The lower layer of structure D would be formed by the lifting of the membrane from the casting plate and acetone egress from the rear.

On the other hand, “swelling” agents lead to a smaller extent of polymer–polymer interactions.<sup>2,36</sup> Thus, the effect of adding “swelling” agents such as  $\text{Mg}(\text{ClO}_4)_2$  is to improve the solvent power of acetone towards CA and to make the intermolecular dissociation more probable. It decreases the dimensions of supermolecular aggregates, which will result in the formation of smaller-size pores,<sup>37,38</sup> and leads to more dilated macromolecular chain average conformation with the result that, in the leaching bath, the desolvation may be uniform. Besides, “swelling” agents bring the solution farther away from the phase separation conditions (Fig. 3). As a direct consequence, increasing amounts of water need to diffuse into the cast film for the phase separation to occur and increasing amounts of solvent would be able to diffuse out before polymer precipitation sets in. Although for the  $\text{Mg}(\text{ClO}_4)_2$  system the rate of solvent outflow is reduced relative to the rate of water flow into the polymer solution, phenomena such as the above and the casting solution viscosity, which acts as a resistance for transfer of solvent and water, result in slow rates of desolvation and precipitation. With respect to membranes prepared under the same conditions from solution containing  $\text{Al}(\text{NO}_3)_3$ , one expects a more marked decrease of the thickness of the immersed film and precipitation from a less dilute solution, which is experimentally confirmed. Membranes cast from solutions containing  $\text{Mg}(\text{ClO}_4)_2$  and immediately leached are thin [74  $\mu\text{m}$  as compared to the casting thickness of 150  $\mu\text{m}$  and the  $\text{Al}(\text{NO}_3)_3$  membrane thickness of 97  $\mu\text{m}$ ], slightly turbid, and mod-



erately swollen [65% in comparison to 72.7% for  $\text{Al}(\text{NO}_3)_3$ -cast membrane] in accordance with the smaller-size of pores. They have a high water permeability and a noticeable salt rejection before heat treatment (Fig. 4).

If casting solutions are prepared with pure water rather than with aqueous salt solutions, the rate of water flow into the cast film will be reduced considerably in the leaching bath. Thus, for systems where there is no inorganic salt, solvent may leave the solution film faster than water enters. Frommer's results<sup>39</sup> indicate that there is effectively no or very low water flow into the cast solutions. Figure 3 shows that the composition will change practically along the line IE and phase separation will occur at a composition similar to that corresponding to point 0. Although the casting solution with 9.99 wt % already contains so much water that only a small amount of acetone has to diffuse out before the boundary line is reached and the membrane sets, the time required for membrane coagulation is long and the cast film shrinks prior to phase separation as indicated by the thinness of resultant membrane (50  $\mu\text{m}$ ). As there is an extensive supermolecular structuralization of these solutions, it results in a closed-cell structure D, whose density is, of course, between that of a dense film and that of an open-cell network.<sup>40</sup> As the membrane structure is practically formed by diffusion of acetone from the CA solution into water, without the intervention of any water penetration, membranes exhibit the same D structure whatever the evaporation time may be (Fig. 6).

Referring to previous data,<sup>1</sup> the addition of 1.11 g KSCN to the casting solution only slightly increases the solvation power for cellulose acetate. As a direct consequence, the viscosity of the casting solution and the water concentration required for precipitation are only slightly increased. Therefore, the morphology of membranes cast from solutions containing 1.11 g KSCN and immediately leached is very similar to that of membranes prepared from saltless solutions. Nevertheless, during the precipitation step, the salt tends to osmotically attract water into the structure and the rate of penetration of water into the cast solution may become large enough to explain the formation of voids and cavities in the upper layer of the membrane. Besides, it renders an account of the tendency for the structure to be C rather than D type [Figs. 8(a) and 12] in this part of the membrane.

### **Effect of Acetone Evaporation Time**

#### *Evaporation Time Shorter Than $t_1$*

Electron micrographs of cross sections of membranes cast from solutions containing  $\text{Al}(\text{NO}_3)_3$  (Fig. 7), KSCN (Fig. 8), or where there is no additive (Fig. 6), and which were allowed to evaporate for a period shorter than  $t_1$  prior to their immersion, exhibit two layers of different structure. Comparison of the rate of acetone evaporation<sup>3</sup> to the rate of thickening of the upper layer, as the air exposure period is increased, shows that the formation of this layer is, at least in part, due to the loss of solvent. The rate of acetone loss is so high that even membranes which were immersed in the water bath within a few seconds from their casting contain a more concentrated and viscous solution at the air-casting solution interface. In addition to the solvent evaporation, transport phenomena during coagulation, that is to say, the penetration of water and the solvent de-

pletion, also contribute to the increase in the polymer concentration in the top layer of the solution. Moreover, upon immersion, owing to the direct contact with the leaching bath, there is a rapid penetration of water and/or solvent depletion at the film surface. These two phenomena make unlikely a liquid-liquid phase separation in the top layer of the solution. Indeed, in this part of the cast film, the system enters the miscibility gap so quickly that there is no time for liquid-liquid phase separation to occur before a high viscosity gel is formed. According to de Gennes<sup>41</sup> and Johnston,<sup>42</sup> under these conditions, the concentration fluctuations which are the subject of the standard treatment of spinodal decomposition are damped by the specific interactions and the segregation of the system into polymer-rich and water-rich phases is hindered. As water progressively diffuses into the gel, the tendency for the system to segregate into two phases and the tendency to provide a continuous assembly of molecules operate in opposite directions. At a certain composition, the first effect slightly prevails, which results in the formation of a more-or-less homogeneous gel with polymer-rich and polymer-poor regions, but at an extremely small scale, since the system remains optically transparent. This polymer matrix is inherently amorphous with a high free volume, and the final structure is the typical B structure which is associated with high water and salt permeability but which is consistent with a noticeable permselectivity after heat treatment. Note that owing to the acetone evaporation, the increase in viscosity at the air-casting solution interface is sufficient to prevent the formation of numerous voids.

Although the solution composition changes along the line IE (Fig. 3) during the air exposure period, in the early stages of evaporation, solvent is lost mainly from the cast film surface. Therefore, in the lower portion of the cast film, the processes taking place upon immersion remain very similar to those occurring in the case of an immediately leached film and the same type of structure is obtained, i.e., type C or D for membranes cast from solutions containing  $\text{Mg}(\text{ClO}_4)_2$ , KSCN, or no additive, respectively. The effect of increased drying time is to cause a thickening of the "B" layer and a thinning of the lower layer.

In order to help readers to better understand which occurs, the concentration profiles of the solvent and nonsolvent in the casting solution at various times during the membrane formation, which were introduced by Strathmann et al.,<sup>22,43</sup> are shown schematically in Figure 16 for the KSCN system.

#### *Evaporation Time Longer Than $t_1$*

In cases where an evaporation step longer than  $t_1$  is involved in the membrane-making procedure, a surface layer is formed before immersion in water, and membranes can be divided into three regions.

**Casting Solutions Containing "Swelling" Agents.** During acetone evaporation, the average composition of the cast solution changes along the line IE, and  $t_1$  sec after casting, the film surface composition path touches the boundary curve. It is immediately apparent from Figure 3 that for casting solutions containing  $\text{Mg}(\text{ClO}_4)_2$  or KSCN, the composition at  $t_1$  is also that at which the sol-gel transition curve crosses the cloud point curve. Thus, for these systems, two processes occur when the evaporation step is equal or longer than  $t_1$ . First, as acetone evaporation proceeds, the surface layer becomes depleted of acetone and, as a consequence, enriched in polymer and aqueous solution of inorganic salt.

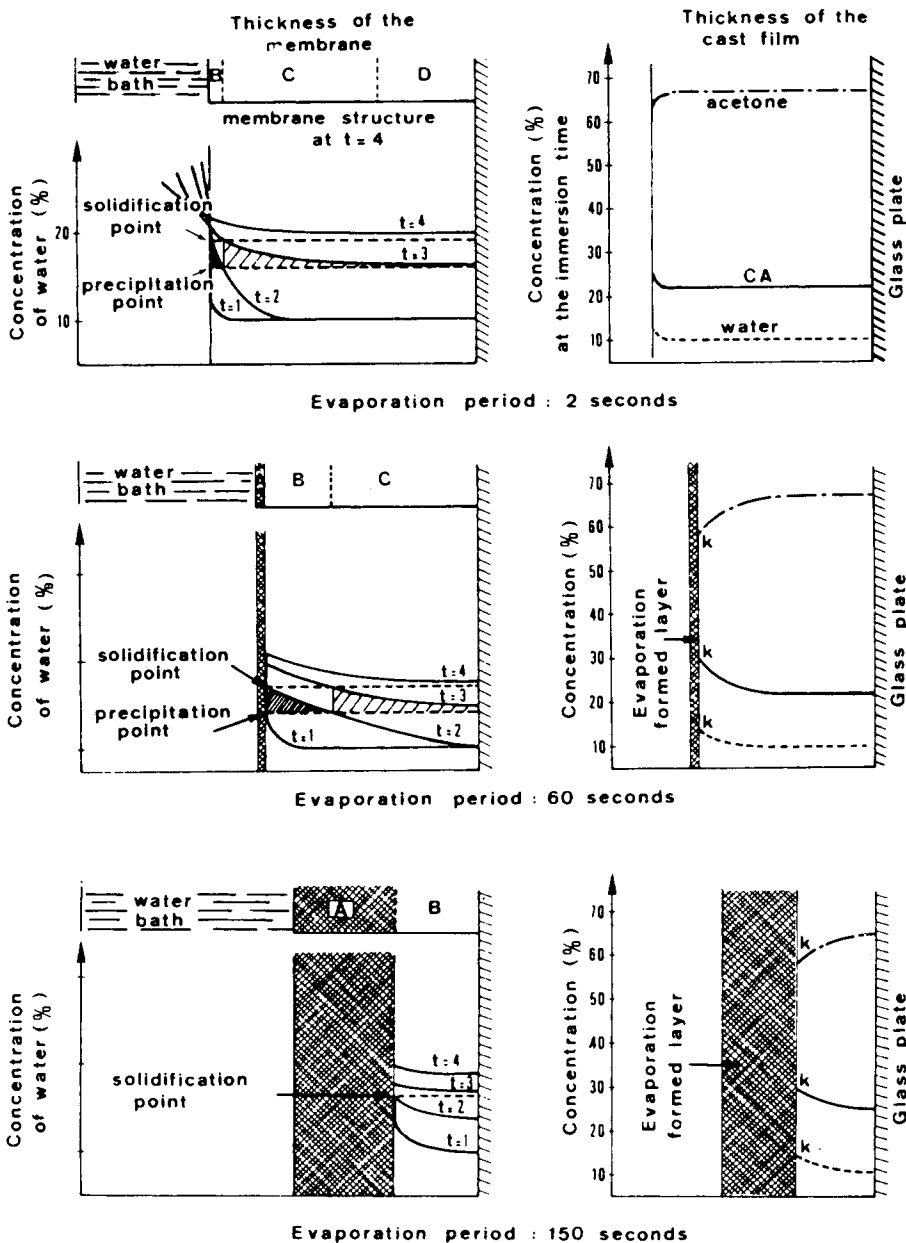


Fig. 16. Concentration profiles in the casting solution containing KSCN at various times during the membrane formation.

As acetone is a good solvent from a thermodynamic point of view, evaporation brings two essential changes in the structure of the surface solution: an increase in polymer concentration and a decrease in polymer-solvent mixture affinity. It results in a solution where the molecules are not swollen or expanded by polymer-solvent interaction but tend rather to form spherical nodules and to gradually aggregate as the proportions of acetone and aqueous solution of inorganic salt change. Then, at  $t_1$ , a sudden gelling occurs when the concentration

of the casting solution becomes sufficiently high for the aggregates to lock into a rigid structure so that there is a sol-gel phase separation analogous to crystallization of supersaturated solution.<sup>30</sup> It results in the formation of an upper layer of structure A. There is an increasing amount of experimental evidence<sup>40,44-46</sup> that the skin thus obtained consists of spherical aggregates called nodules.

When the film is then immersed in the water bath, water diffuses through this evaporation-formed layer and causes the subsequent coagulation of the sublayer, producing a structure of B type and, from the dilute CA solution at the lower layer, a D and/or C structure [Figs. 8(d) and 9]. The effect of increased drying time is to cause a thickening of the evaporation-formed A layer and the B "sublayer" until they extend the full thickness of the membrane ( $t = 120$  sec). In addition, owing to the progressive decrease in solvent concentration, the lower layer is produced from a more and more concentrated polymer solution and there is a gradual decrease in pore size until the membrane contains no large pores. As a direct consequence, membranes change from opaque and nonuniform to turbid and then transparent.

In cases where an evaporation step longer than  $t_2$  (180 sec) is involved in the membrane-making procedure, the membrane is completely formed by evaporation prior to contact with water. A dense, symmetrical membrane of structure A is obtained [Fig. 8(f)].

Although the pressure effects discussed in ref. 47 should be taken into account, such a morphological model may be tested against the data presented in Figure 5 concerning the influence of an air exposure period on the desalination characteristics of membranes prepared from systems containing KSCN.

It can be seen that an increase in the air exposure period prior to contact with water first improves the hydraulic permeability and decreases the permselectivity of the "as cast" membranes until the evaporation time reaches 110-120 and 60 sec, respectively. Such a behavior must be associated with the gradual development of structure B at the expense of structures C and D. Indeed, whereas the closed-pore structure D gives rise to an important resistance to transport, structure C and, to a greater extent, structure B are consistent with water and salt permeability.

At time  $t_1$ , a layer of structure A appears at the film surface. The extent to which the aggregation has proceeded by the time gelation occurs largely determines the porosity of structure A. However, as this upper layer is produced from a more concentrated polymer solution than the sublayer, it has a lower porosity and, consequently, a lower hydraulic permeability and a better permselectivity. Further evaporation from the set gel, accompanied by shrinkage of the gel when it is immersed in water, results in a decrease in the porosity of the upper layer of structure A. Therefore, as soon as the evaporation period involved in the membrane-making procedure reaches 60 sec, there is an increase in the salt rejection.

As shown by electron microscopy (Fig. 9), the main morphological change in the range of evaporation times 60-120 sec is the development of structure B at the expense of structure C. Indeed, the upper layer of structure A remains thin ( $t = 120$  sec,  $e_A = 2 \mu\text{m}$ ,  $e_B = 42 \mu\text{m}$ ). As the water permeability of structure B is higher than that of structure C,<sup>23</sup> the flow rate continues to increase contrary to the permselectivity. Then, the increase in the thickness of the upper layer

of structure A, which grows faster for evaporation periods longer than 110–120 sec ( $t = 120$  sec;  $e_A$ : 4.5%,  $e_B$ : 95.5%,  $t = 150$  sec,  $e_A = 54.8%$ ,  $e_B = 45.2%$ ) contributes to the decreased flow rates observed in cases where an evaporation step longer than 120 sec is involved in the membrane-making procedure.

Figure 5 shows that membranes dried for 120–240 sec are the only ones consistent with both high permeability and high permselectivity after heat treatment. Indeed, for membranes made using short evaporation times, the rigid nature of the membrane matrix in the layer of structure D owing to the thick dense interpore walls, makes unlikely the reorganization of long parts of CA chains by heat treatment. In the same way, when the evaporation step is longer than  $t_2$ , it results in a considerably dense membrane which is little influenced by heat treatment.

The effect of the evaporation step on desalination characteristics of membranes cast from solutions containing  $\text{Mg}(\text{ClO}_4)_2$  (Fig. 4) is very similar to that observed for membranes cast from solutions containing KSCN. This suggests that the formation of  $\text{Mg}(\text{ClO}_4)_2$  membranes is consistent with the phase separation processes discussed in the case of KSCN membranes. However, as mentioned in the first part of the discussion, the effects of  $\text{Mg}(\text{ClO}_4)_2$  on the casting solution structure, the phase diagram, and the transport phenomena during coagulation are different from those of KSCN, so that the structure of the lower layer is rather of type C even at short evaporation times and the pore size in the C layer is smaller, which makes the differentiation between the evaporation formed layer, the “sublayer,” and the lower layer more difficult.

**Casting Solution without an Additive or with a Gelling Agent— $\text{Al}(\text{NO}_3)_3$ .** For systems containing  $\text{Al}(\text{NO}_3)_3$ , only a small amount of acetone has to be evaporated before the boundary curve is reached [11.9% in comparison with 18.8% for the KSCN system and 20.9% for the  $\text{Mg}(\text{ClO}_4)_2$  system] so that the evaporation time at which CA precipitation begins at the cast film surface is relatively short:  $t_1 = 40$  sec. Figure 3 shows that in the upper portion of the cast film, phase separation occurs at a composition corresponding to point a, which is very close to point 0 determined for saltless systems. In addition, as acetone evaporates, the “gelling” agent  $\text{Al}(\text{NO}_3)_3$  concentration increases, leading to a greater attractive force between CA chains and a higher amount of supermolecular aggregates.<sup>2</sup> Under these conditions, the evaporation-formed layer is of D type [Fig. 7(c)]. As a direct consequence at time  $t_1$  one notices a sharp decrease in the membrane hydraulic permeability (Table I). The effect of increased drying time is to cause a gradual thinning of the B sublayer and the C lower layer and a thickening of the D upper layer until it extends to the full thickness of the membrane ( $t_2 = 120$  sec). This results in the formation of practically impermeable membranes.

## CONCLUSIONS

Experimental investigations reported in this article have allowed us to establish that in order to obtain structures consistent with both high permeability and high permselectivity after heat treatment, hence useful for reverse osmosis, the casting solution composition and the membrane-making procedure must be such that:

(1) the solvation of CA chains as well as the casting solution viscosity is noticeable;

(2) the CA precipitation requires a relatively high amount of water; and  
 (3) the polymer concentration in the casting solution is high enough and the evaporation time is long enough to obtain a "surface layer" brought about by a gradual aggregation and a sudden gelling owing to solvent evaporation and a sublayer related to the quite distinct phenomena of coagulation in water.

On the other hand, spongelike structures suitable for ultrafiltration can be obtained by lowering the solvent power of the acetone-water-inorganic salt combination towards CA. Indeed, such structures are associated with a fast liquid-liquid phase separation from casting solutions of low viscosity.

The authors wish to thank La Direction des Recherches et Moyens d'Essais and La Délégation Générale à la Recherche Scientifique et Technique for supporting this work. The authors are also indebted to the Fondation Jean Langlois for a generous donation. They are also grateful to one referee for the care and thoroughness with which he reported.

### References

1. J. L. Halary, C. Noël, and L. Monnerie, *Desalination*, **13**, 251 (1973).
2. J. Vinit, C. Noël, and L. Monnerie, *Desalination*, **15**, 267 (1974).
3. J. Vinit, J. L. Halary, C. Noël, and L. Monnerie, *Eur. Polym. J.*, **11**, 71 (1975).
4. S. Loeb and S. Sourirajan, *Adv. Chem. Ser.*, **38**, 117 (1962).
5. B. Kunst and S. Sourirajan, *J. Appl. Polym. Sci.*, **14**, 1983 (1970).
6. R. Pilon, B. Kunst, and S. Sourirajan, *J. Appl. Polym. Sci.*, **15**, 1317 (1971).
7. B. Kunst, A. M. Basnec, and G. Arneri, *4th International Symposium on Fresh Water from the Sea, Heidelberg*, **4**, 217 (1973).
8. G. J. Gittens, P. A. Hitchcock, D. C. Sammon, and G. E. Wakley, *Desalination*, **8**, 369 (1970).
9. G. J. Gittens, P. A. Hitchcock, and G. E. Wakley, *Desalination*, **12**, 315 (1973).
10. M. A. Frommer and R. Matz, Office of Saline Water, Res. Dev. Prog. Rept. No. 774, May 1972.
11. H. Strathmann, P. Scheible, and R. W. Baker, *J. Appl. Polym. Sci.*, **15**, 811 (1971).
12. M. N. Sarbolouki, *J. Polym. Sci. Polym. Lett., Ed.* **11**, 753 (1973).
13. M. T. So, F. R. Eirich, R. W. Baker, and H. Strathmann, *J. Polym. Sci. Polym. Lett. Ed.* **11**, 201 (1973).
14. S. D. Hong and C. M. Burns, *J. Appl. Polym. Sci.*, **15**, 1995 (1971).
15. C. Lemoine, Thèse d'Ingénieur Docteur, Paris, CNRS-A.O. 12828, 1976.
16. M. A. Frommer, and D. Lancet, *J. Appl. Polym. Sci.*, **16**, 1295 (1972).
17. Y. Taniguchi and S. Horigome, *J. Appl. Polym. Sci.*, **19**, 2743 (1975).
18. H. G. Burghoff and W. Pusch, *J. Appl. Polym. Sci.*, **23**, 473 (1979).
19. I. I. Ryskina and V. M. Aver'yanova, *Polym. Sci., USSR*, **13**, 2457 (1971).
20. A. Takahashi, T. Kawaharada, and T. Kato, *Polym. J.* **11**, 671 (1979); *Polym. J.*, **3**, 207 (1972).
21. L. Broens, F. W. Altena, C. A. Smolders, and D. M. Koenhen, *Desalination*, **32**, 33 (1980).
22. H. Strathmann, K. Kock, P. Amar, and R. W. Baker, *Desalination*, **16**, 179 (1975).
23. J. L. Halary, C. Noël, and L. Monnerie, *J. Appl. Polym. Sci.*, **24**, 985 (1979).
24. M. A. Frommer and D. Lancet, in *Reverse Osmosis Membrane Research*, H. Lonsdale and H. E. Podall, Eds., Plenum, New York, 1972, p. 85.
25. M. Guillotin, C. Lemoine, C. Noël, and L. Monnerie, *Desalination*, **21**, 165 (1977).
26. R. Matz, *Desalination*, **10**, 1 (1972).
27. M. A. Frommer and R. M. Messalem, *Ind. Eng. Chem. Prod. Res. Develop.*, **12**, 328 (1973).
28. J. G. Helmcke, *Kolloid Z.*, **135**, 101 (1954).
29. V. Gröbe, G. Mann, and G. Duwe, *Faserforsch. Textiltech.*, **17**, 142 (1966).
30. D. M. Koenhen, M. H. V. Mulder, and C. A. Smolders, *J. Appl. Polym. Sci.*, **21**, 199 (1977).
31. A. Driancourt, Thèse de 3ème Cycle, Paris, 1976.
32. M. A. Frommer, R. Matz, and U. Rosenthal, *Ind. Eng. Chem., Prod. Res. Dev.*, **10**, 193 (1971).
33. M. A. Kraus, M. Nemas, and M. A. Frommer, *J. Appl. Polym. Sci.*, **23**, 445 (1979).
34. M. A. Frommer, I. Feiner, O. Kedem, and R. Bloch, *Desalination*, **7**, 393 (1970).

35. P. M. Fahey and H. E. Grethlein, *Desalination*, **9**, 297 (1971).
36. R. E. Kesting, *J. Appl. Polym. Sci.*, **9**, 663 (1965).
37. L. Pageau and S. Sourirajan, *J. Appl. Polym. Sci.*, **16**, 3185 (1972).
38. R. E. Kesting, *Synthetic Polymeric Membranes*, McGraw-Hill, New York, 1971, chap. 5.
39. M. A. Frommer and D. Lancet, *Polym. Prepr. Am. Chem. Soc. Div. Polym. Chem.*, **12**, 245 (1971).
40. R. E. Kesting, *J. Appl. Polym. Sci.*, **17**, 1771 (1973).
41. P. G. de Gennes, Lectures given at Collège de France, Paris, 1979, in *Scaling Concepts in Polymer Physics*, P. G. de Gennes, Ed., Cornell U. P., Ithaca, NY, 1979, p. 151.
42. G. J. Johnston, *Polymer*, **19**, 228 (1978).
43. H. Strathmann and K. Kock, *Desalination*, **21**, 241 (1977).
44. R. D. Schulz and S. K. Asunmaa, *Rec. Prog. Surface Sci.*, **3**, 291 (1970).
45. M. Panar, H. H. Hoehn, and R. R. Hebert, *Macromolecules*, **6**, 777 (1973).
46. R. D. Sanderson and H. S. Pienaar, *Desalination*, **25**, 281 (1978).
47. J. L. Halary, C. Noël, and L. Monnerie, *Desalination*, **27**, 197 (1978).

Received July 1, 1977

Accepted January 23, 1980